Magn Reson Med Sci 2021; 20; 253–263
doi:10.2463/mrms.mp.2020-0060
Published Online: August 12, 2020

MAJOR PAPER

Radiomics Analysis of Susceptibility Weighted Imaging for Hepatocellular Carcinoma: Exploring the Correlation between Histopathology and Radiomics Features

Zhijun Geng[1,2†], Yunfei Zhang[3†], Shutong Wang[4], Hui Li[1,2], Cheng Zhang[1,2], Shaohan Yin[1,2], Chuanmiao Xie[1,2*], and Yongming Dai[3]

Purpose: No previous researches have extracted radiomics features from susceptibility weighted imaging (SWI) for biomedical applications. This research aimed to explore the correlation between histopathology of hepatocellular carcinoma (HCC) and radiomics features extracted from SWI.

Methods: A total of 53 patients were ultimately enrolled into this retrospective study with MR examinations undertaken at a 3T scanner. About 107 radiomics features were extracted from SWI images of each patient. Then, the Spearman correlation test was performed to evaluate the correlation between the SWI-derived radiomics features and histopathologic indexes including histopathologic grade, microvascular invasion (MVI) as well as the expression status of cytokeratin 7 (CK-7), cytokeratin 19 (CK-19) and Glypican-3 (GPC-3). With SWI-derived radiomics features utilized as independent variables, four logistic regression-based diagnostic models were established for diagnosing patients with positive CK-7, CK-19, GPC-3 and high histopathologic grade, respectively. Then, receiver operating characteristic analysis was performed to evaluate the diagnostic performance.

Results: A total of 11, 32, 18 and one SWI-derived radiomics features were significantly correlated with histopathologic grade, the expression of CK-7, the expression of CK-19 and the expression of GPC-3 ($P < 0.05$), respectively. None of the SWI-derived radiomics features was correlated with MVI status. The areas under the curve were 0.905, 0.837, 0.800 and 0.760 for diagnosing patients with positive CK-19, positive CK-7, high histopathologic grade and positive GPC-3.

Conclusion: Extracting the radiomics features from SWI images was feasible to evaluate multiple histopathologic indexes of HCC.

Keywords: *susceptibility weighted imaging, radiomics analysis, hepatocellular carcinoma, histopathology*

Introduction

With the seventh incidence and the third leading cause of cancer-related mortality,[1] hepatocellular carcinoma (HCC) has been a huge threat to human health for a long time. The marked heterogeneous nature of HCC causes great difficulties for the establishment of personalized clinical management. Thus, there is a growing evidence that it is necessary for comprehensively characterizing HCC according to the different histopathologic features. Comprehensive insights from histopathologic features are conducive to guide the following diagnosis, therapy, prognosis prediction and so on. For example, HCCs with positive cytokeratin 19 (CK-19) always indicates a high rate of recurrence, poor prognosis and a high probability of lymph node metastasis.[2] Abnormal expression of cytokeratin 7 (CK-7) suggests the aggressive biological behavior of HCC.[3] Moreover, it was recently reported that Glypican-3 (GPC-3), a star molecule, can be a novel target for the treatment of HCC.[4] Besides, histopathologic grade, microvascular invasion (MVI) and so on are also the important independent prognostic factors. High histopathological

[1]State Key Laboratory of Oncology in South China, Collaborative Innovation Center for Cancer Medicine, Sun Yat-sen University Cancer Center, Guangzhou, China
[2]Department of Radiology, Sun Yat-sen University Cancer Center, Guangzhou, China
[3]Central Research Institute, United Imaging Healthcare, Shanghai, China
[4]Department of Hepatic Surgery, First Affiliated Hospital of Sun Yat-sen University, Guangzhou, Guangdong, China

*Corresponding author: Department of Radiology, State Key Laboratory of Oncology in Southern China, Sun Yat-sen University Cancer Center, No. 651, Dongfeng East Road, Guangzhou 510060, China. E-mail: xiechuanmiao111@163.com

†These authors contributed equally to this work.

Received: April 16, 2020 | Accepted: May 30, 2020

grade and MVI always indicate a poor clinical outcome.[5,6] Therefore, unveiling the histopathologic characteristics is of extreme significance for guiding the subsequent clinical management of HCC. However, histopathological examination, the gold standard of assessing histopathologic features, has several disadvantages including invasive sampling, potential sampling bias, time consumption and so on.

In the past few years, evaluating the histopathology via MRI has attracted a lot of research attention because of the complementary superiorities such as non-invasive measurement, cost-effective character and so on.[7–10] By means of sensing the susceptibility differences caused by "intrinsic contrast agents" containing deposited iron, hemoglobin, hemosiderin, susceptibility weighted imaging (SWI) has evolved as an emerging MRI technique for characterizing HCC with unique image contrast due to the additional phase information.[11]

Recently, able to extract thousands of quantitative image features, the state-of-the art radiomics technology helps pave the unprecedented way for reflecting the underlying pathology via capturing the pathology-related image manifestations invisible to the naked eyes.[12] However, there are very limited number of researches aiming to utilize MRI radiomics features for evaluating the multiple histopathologic characteristics of HCC. Moreover, many important histopathologic characteristics such as CK-19, GPC-3, MVI and so on were not simultaneously assessed.

To the best of our knowledge, no previous researches have extracted radiomics features from SWI for biomedical applications. Thus, this research aims to explore the correlations between the SWI-derived radiomics features and multiple histopathologic features of HCC including MVI, CK-7, CK-19, GPC-3 and histopathologic grade.

Materials and Methods

Patients

The approval from the local Institute Review Board was successfully obtained. Written informed consent from each patient was waived because of the nature of retrospective study. The inclusion and exclusion criteria were respectively listed as follows:

Inclusion criteria

(1) Patients suspected as HCC according to the previous image examination.
(2) Patients underwent liver MRI and subsequent surgery.

Exclusion criteria

(1) Pathologically proved not to be HCC.
(2) Pre-operative treatment such as percutaneous ethanol injection, radiofrequency ablation, chemoembolization and the combination of above.
(3) Poor image quality caused by metal or motion artifact.
(4) Tumor <1 cm.
(5) Lack of complete pathological results.

MR examinations

All the MR examinations were performed with a commercial 3T MR scanner (uMR 780; United Imaging Healthcare, Shanghai, China) with a 12-channel body coil. Clinical routine MR protocols contained a T_2-weighted (T_2W) fast spin echo (FSE) sequence, a T_1-weighted (T_1W) 3D gradient echo (GRE) sequence, a T_1W dual-echo (in and out phase) 3D GRE sequence, an echo planar imaging (EPI) based spin echo sequence for diffusion weighted imaging (DWI). For SWI, a 2D breath-hold GRE sequence was utilized. The detailed parameters of above MR sequences were shown in Table 1.

Pathologic examination

All the histopathological features including histopathologic grade, MVI status and the expression of CK-7, CK-19 and Glypican-3 were obtained in electronic medical record system at our institute. Standard clinical histopathologic evaluation was performed by two experienced pathologists with more than 5 years' experience. In detail, histopathological grade and MVI status were assessed via reviewing the H&E stained specimens. The other immunohistochemical features were assessed via immunohistochemically staining with specific monoclonal antibodies. Then, stained HCC sections were carefully evaluated with an optical microscope to

Table 1 MR Protocols

Sequence	TR (ms)	TE (ms)	FA (°)	Section thickness (mm)	Matrix	FOV (mm^2)
T_2-weighted FSE	3286.0	82.0	120	5	320 × 320	380 × 380
T_1-weighted 3D GRE	3.3	1.5	10	2	280 × 400	280 × 380
T_1-weighted dual-echo 3D GRE	4.1	1.3/2.6	10	2	268 × 480	300 × 380
EPI–DWI (b = 0, 200 and 800 s/mm^2)	4281.0	68.5	90	5	202 × 256	300 × 380
SWI	142.3	10.0	30	5	216 × 368	280 × 380

DWI, diffusion weighted imaging; EPI, echo planar imaging; FSE, fast spin echo; GRE, gradient echo; SWI, susceptibility weighted imaging.

conclude the expression status [positive (+) or negative (−)] of immunohistochemical features. It should be noted that in order to eliminate the false-negative evaluation, 5% was utilized as a cut-off value for determining the CK-19 status (CK-19 positive: ≥5% of tumor cells and CK19 negative: <5% of tumor cells).[13] Similarly, with previous researches as the references, the GPC-3 expression was determined as positive if the percentage of immunoreactive cells was greater than 10% of the tumor cells.[14,15] According to the previous reports, CK-7 expression was determined as positive when the percentage of immunoreactive cells was greater than 5% of the tumor cells.[16,17]

Radiomics features

***Image segmentation*:** The image segmentation was performed with an open-source commercial software named 3D Slicer (https://www.slicer.org) by two radiologists respectively having 9 and 12 years of experience. Volume of interests (VOIs) were defined by manually outlining the tumor border in SWI images with the T_2-weighted imaging (T_2WI) images as the references. For each HCC, the whole tumor was incorporated into the VOI.

Calculation of radiomics features: Radiomics features in segmented tumors were automatically calculated with Pyradiomics 1.3.0 (https://pyradiomics.readthedocs.io/en/latest/), an open-source software based on python.[18] Pyradiomics provides seven categories of features including first-order features (first order: 18 features), shape-based features (shape: 14 features), gray level co-occurence matrix features (GLCM: 24 features), gray level run length matrix features (GLRLM: 16 features), gray level size zone matrix (GLSZM: 16 features), neighboring gray tone difference matrix (NGTDM: five features) and gray level dependence matrix (GLDM: 14 features). The detailed list of radiomics features and their mathematical implications were available in the homepage of Pyradiomics.

Features selection: The intra-class coefficients (ICCs) of the measurements from two radiologists were applied to evaluate the reliability and reproducibility of radiomics features. The features with ICCs of <0.75 were eliminated because of low reproducibility and reliability. Then, for the retained radiomics features, the measurements of two observers were averaged.

Statistical analysis

Spearman correlation test was performed to evaluate the correlation between the radiomics and histopathologic features. Then, the radiomics features significantly correlated with histopathological features were regarded as candidate features for establishing the diagnostic models. Next, binary logistic regression models were established for evaluating the status of histopathologic features with the candidate features. For example, there were 32 radiomics features significantly correlated with the expression of CK-7. The logistic regression-based model for discriminating patients with positive CK-7 from patients with negative CK-7 was established with 32 candidate radiomics features. Then, the diagnostic power of logistic regression-based model was determined by receiver operating characteristic (ROC) analysis. All the statistical analyses were performed with the SPSS 26.0 (IBM, Chicago, IL, USA), software R (version 3.6.2; The R fundation for statistical computing, Vienna, Austria) and MedCale 15.0 (MedCalc Software, Ostend, Belgium). Two-sided *P*-values of <0.05 were regarded as having statistical difference.

Results

Clinical and imaging characteristic

From January to December 2019, 84 patients suspected as HCC were enrolled into this study. Then, 31 patients were excluded including patients pathologically confirmed as other hepatic malignancy (n = 9, 4 cases of cholangiocarcinoma, 3 cases of mixed HCC and cholangiocarcinoma, 2 cases of metastases), patients with pre-operative treatment (n = 10), poor image quality (n = 3), patients with absence of pathological results required for this study (n = 9), which resulted in that a total of 53 patients (male: 52, female: 1, median age: 53.0 years) were ultimately introduced into this study. The detailed clinical characteristics were displayed in Table 2. Representative MR images and immunohistochemical staining specimens of two patients with different histopathological features were shown in Figs. 1–4 and SF1. With regard to representative images of a patient with low grade HCC as well as negative status of MVI, GPC-3, CK-7 and CK-19 in Fig. 1, SWI images of another patient with high grade HCC as well as positive status of MVI, GPC-3, CK-7 and CK-19 in Fig. 2 displayed that there existed some irregular hypo-signal intensities within the tumor lesion. In detail, multiple patchy areas with hypointense on SWI images were identified, which indicated the existence of some blood products within the lesion. Moreover, there were also multiple linear hypointense on SWI images within the lesion that serving as the image manifestations of hypervascularity. According to the previous researches, irregular hypo-signal intensities within the tumor lesion were caused by the extra dephasing effect because of intra-tumoral hemorrhage, hypervascularity and so on.[19,20] The resected liver specimen in Fig. 4e showed the micro-hemorrhage and so on which were the physiological basis of image manifestations of SWI in Fig. 2. Quite differently, except uniform signal intensity within tumor lesion, no irregular or abnormal image manifestations of two patients were identified through DWI image and T_2WI image of two patients.

Correlations between the SWI radiomics features and histopathological indexes

According to the reliability analysis with ICCs, two radiomics features were excluded because of the ICCs of smaller than 0.75. The ICCs of all the other 105 radiomics features were larger than 0.75, which proved the relatively satisfying data reliability. The statistical results indicated that SWI-derived

Table 2 Clinical characteristics

Characteristics	Values
Mean age (years)	52.4 ± 10.4 (Min: 32, Max: 74, Median: 53.0)
Gender	
Men	52
Women	1
Size of tumor (mm)	43.6 ± 20.3 (Min: 11.0, Max: 112.0)
AFP (ng/mL)	4006.0 ± 13756.5
Ki67 (%)	23.2 ± 17.2 (Min: 1, Max: 70)
PIVKA-II (mAU/mL)	205.00 (Min: 23.0, Max: 54864.0)
Background liver and etiology	
Hepatitis B virus	53
Cirrhosis	26
Non-cirrhosis	27
Histopathological grade	1–4
Low grade (E-S 1 and E-S 2)	30
High grade (E-S 3 and E-S 4)	23
Glypcian-3	
Positive	40
Negative	13
CK-7	
Positive	30
Negative	23
CK-19	
Positive	16
Negative	37
MVI	
Positive	20
Negative	33
Capsule formation	
With	23
Without	30
Satellite lesions	
With	1
Without	52

AFP, alpha-fetoprotein; CK-7, cytokeratin 7; CK-19, cytokeratin 19; MVI, microvascular invasion; PIVKA-II, protein induced by vitamin K absence or antagonist-II.

radiomics features were significantly associated with various histopathological characteristics. Specifically, there were 11, 18, one and 32 radiomics features significantly correlated with the status of histopathologic grade, CK-19 expression, GPC-3 expression as well as CK-7 expression. However, none of the SWI-derived radiomics features displayed significant correlations with the MVI. Detailed correlation coefficients and significance level were displayed in Tables 3 and 4. In total, there were 62 radiomics features showing significant correlations with the histopathological features studied in this research. As Fig. 5 exhibited, among these radiomics features, the number of GLCM features was the largest (21, 33.9%), followed by the number of GLRLM features (13, 21.0%), the number of first-order features (13, 20.9%), the number of GLSZM features (6, 9.7%), the number of GLDM features (5, 8.1%), the number of NGTDM features (3, 4.8%) and the number of shape features (1, 1.6%).

Diagnostic performance evaluation

Four binary logistic regression-based diagnostic models were established via introducing the SWI-derived radiomics features significantly correlated with specific histopathological indexes. The ROC curves in Fig. 6 indicated that the diagnostic model utilized for distinguishing the patients with positive CK-19 (LG_{CK-19}) achieved the AUC of 0.905 [95% confidence interval (CI): 0.793–0.969]. Besides, the AUC of the model for diagnosing patients with positive CK-7 (LG_{CK-7}) was 0.837 (95% CI: 0.710–0.924) followed by the AUC of model for diagnosing patients with high grade HCC (LG_{grade}) (AUC = 0.800, 95% CI: 0.667–0.897) and the AUC of model for diagnosing patients with positive GPC-3 (LG_{GPC-3}) (AUC = 0.760, 95% CI: 0.623–0.866). Since there were no significant correlations between the SWI-derived radiomics features and MVI status, the diagnostic model was not established for discriminating the patients with MVI(+) from patients with MVI(−). Detailed quantitative indexes of diagnostic performance were displayed in Table 5.

Discussion

This study first made an attempt to evaluate the feasibility of exploring the correlation between SWI radiomics features and histopathological characteristics of HCC. To the best of our knowledge, no previous researches have extracted radiomics features from SWI for biomedical applications. There was only one very recent research aiming to evaluate the clinical potential of texture features extracted from SWI.[21] Lee et al. performed the texture analysis on SWI to evaluate the deep medullary veins. However, with regard to radiomics analysis conventionally providing hundreds of quantitative features, only three first-order parameters: entropy, skewness and kurtosis were utilized for differentiating infants with ischemic injury. Differently, in this study, a total of 107 quantitative features were obtained from SWI images of each patient. A lot more radiomics markers held great potential for providing more diagnostic predictors.

Unveiling the histopathologic characteristics of HCC including histopathologic grade,[6] MVI,[22] the expression of Ki67,[23] the expression of AFP[24] and so on with image features has attracted innumerable research attention because it is extremely important for comprehensively characterizing tumor from different perspectives. However, (1) very limited

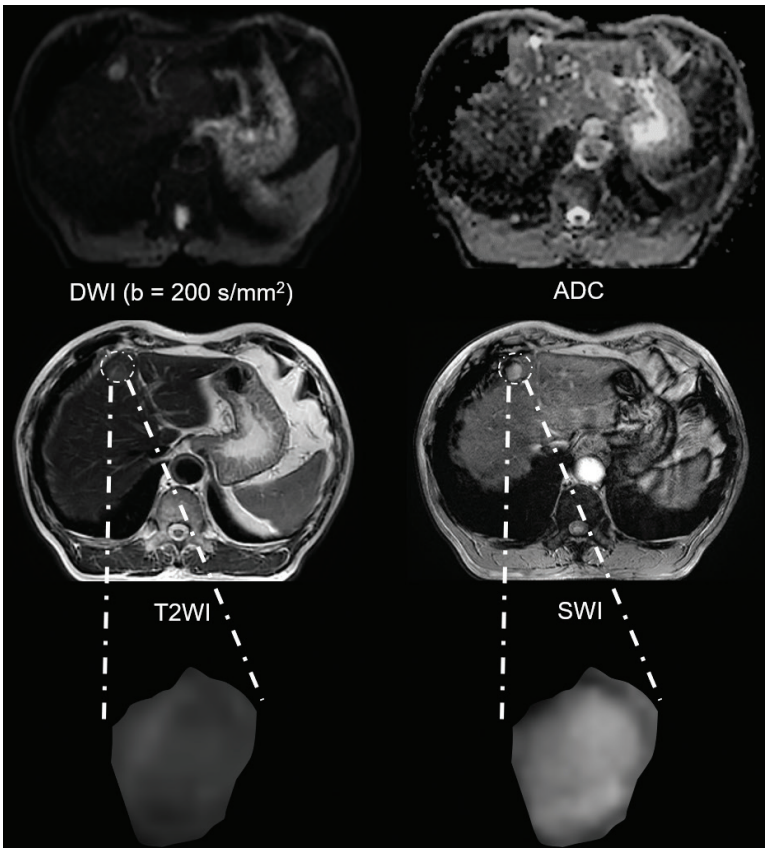

Fig. 1 The MR images including DWI image (b = 200 s/mm^2), ADC map, T_2WI image and SWI image of one patient with low grade HCC, negative status of MVI, GPC-3, CK-7 and CK-19. ADC, apparent diffusion coefficient; CK-7, cytokeratin 7; CK-19, cytokeratin 19; DWI, diffusion weighted imaging; GPC-3, Glypican-3; HCC, hepatocellular carcinoma; MVI, microvascular invasion; SWI, susceptibility weighted imaging; T_2WI, T_2- weighted imaging.

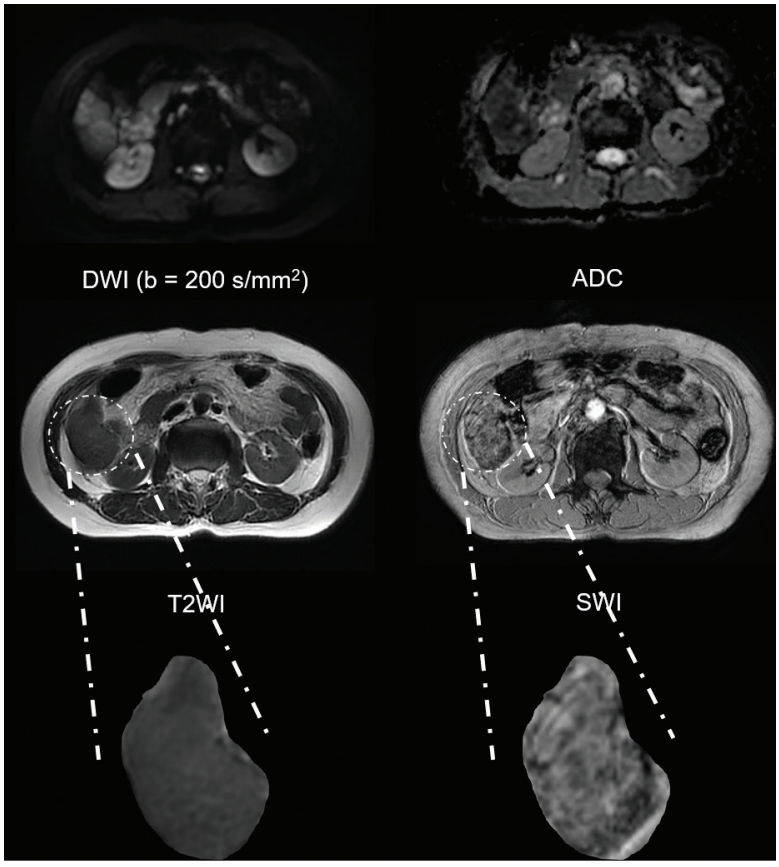

Fig. 2 The MR images including DWI image (b = 200 s/mm^2), ADC map, T_2WI image and SWI image of one patient with high grade HCC, positive status of MVI, GPC-3, CK-7 and CK-19. ADC, apparent diffusion coefficient; CK-7, cytokeratin 7; CK-19, cytokeratin 19; DWI, diffusion weighted imaging; GPC-3, Glypican-3; HCC, hepatocellular carcinoma; MVI, microvascular invasion; SWI, susceptibility weighted imaging; T_2WI, T_2-weighted imaging.

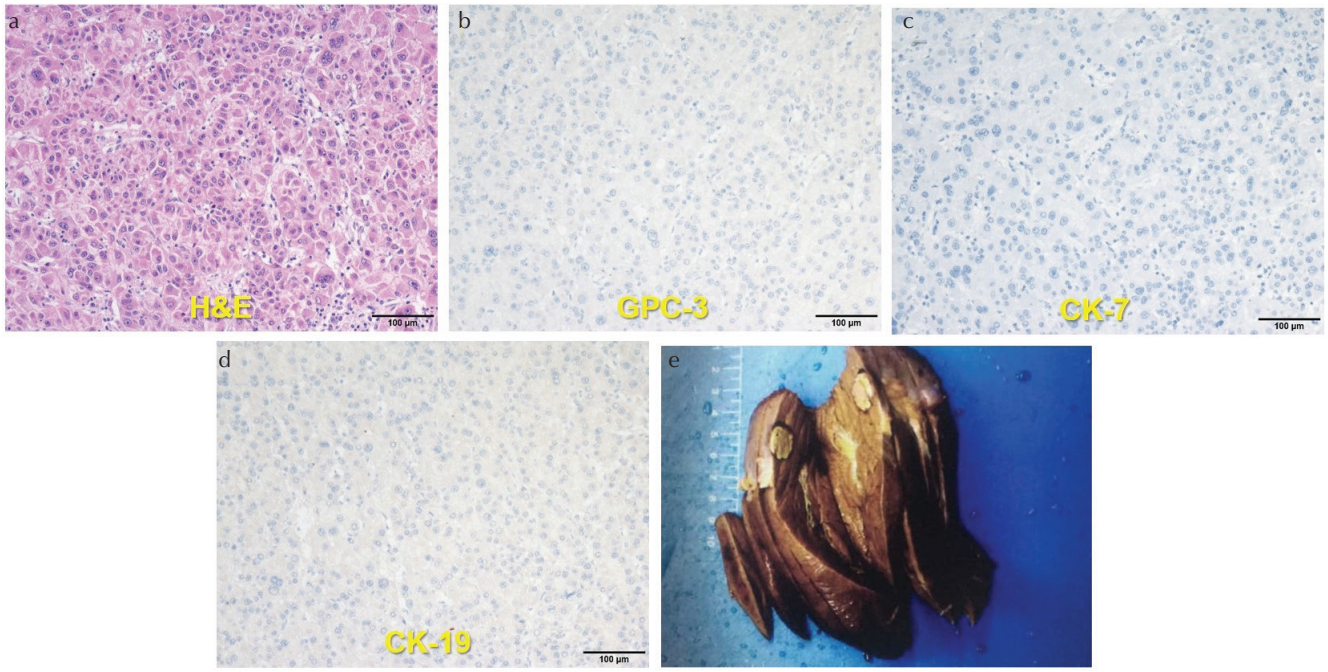

Fig. 3 Histopathologic and immunohistochemical photomicrographs (×200) of one patient whose MR images are displayed in Fig. 1. (**a**) H&E stained section (low grade, without MVI), (**b**) GPC-3 stained section (GPC-3 expression: negative), (**c**) CK-7 stained section (CK-7 expression: negative), (**d**) CK-19 stained section (CK-19 expression: negative) and (**e**) surgical specimen (*Note*: There was no micro-hemorrhage according to the specimen.). CK-7, cytokeratin 7; CK-19, cytokeratin 19; GPC-3, Glypican-3; MVI, microvascular invasion.

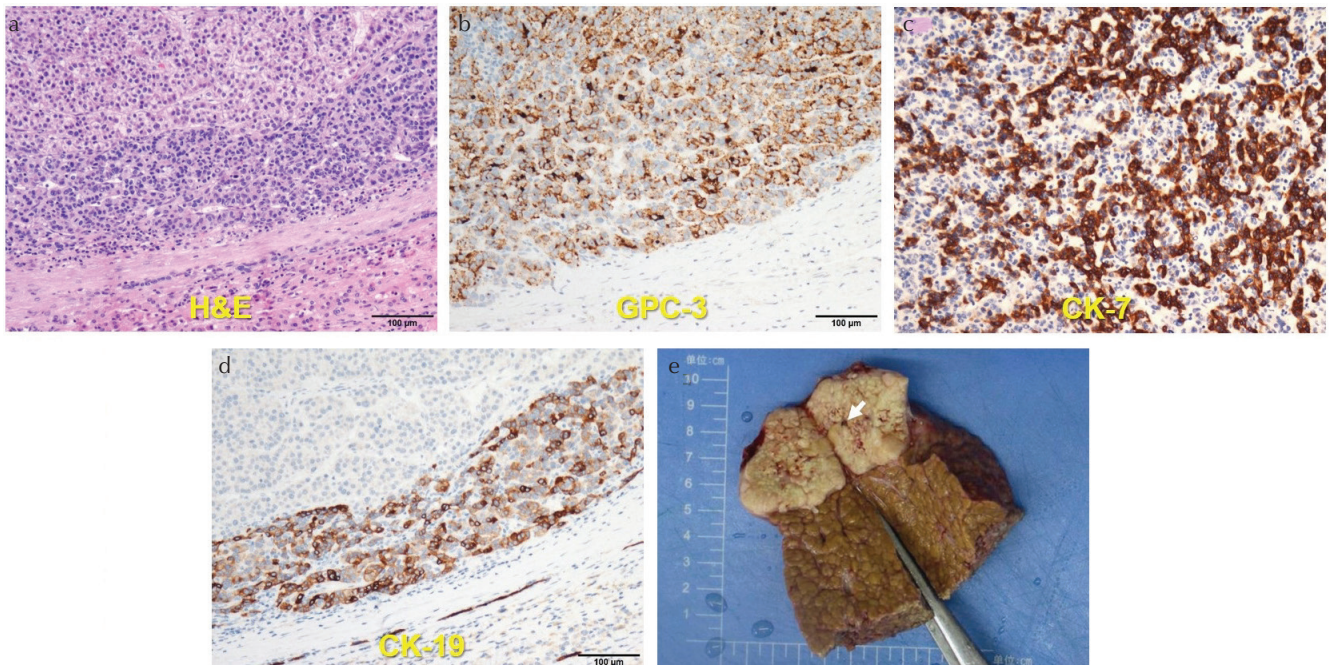

Fig. 4 Histopathologic and immunohistochemical photomicrographs (×200) of one patient whose MR images are displayed in Fig. 2. (**a**) H&E stained section (high grade, with MVI), (**b**) GPC-3 stained section (GPC-3 expression: positive), (**c**) CK-7 stained section (CK-7 expression: positive), (**d**) CK-19 stained section (CK-19 expression: positive) and (**e**) surgical specimen (*Note*: the micro-hemorrhage was indicated by the *white arrow*). CK-7, cytokeratin 7; CK-19, cytokeratin 19; GPC-3, Glypican-3; MVI, microvascular invasion.

Table 3 SWI-derived radiomics features which were significantly correlated with tumor grade as well as the status of CK-19 and GPC-3

Radiomics features	*r*	*P*
Grade		
Kurtosis	0.361	0.008
Idmn	0.326	0.017
Idn	0.346	0.011
Gray level non-uniformity	0.294	0.033
Large dependence high gray level emphasis	0.304	0.027
Gray level non-uniformity	0.279	0.043
Large area emphasis	0.316	0.021
Large area high gray level emphasis	0.333	0.015
Zone variance	0.319	0.020
Contrast	–0.363	0.007
Maximum 2D-diameter row	0.271	0.049
GPC-3		
Dependence non-uniformity normalized	–0.387	0.004
CK-19		
10th percentile	0.410	0.002
Kurtosis	0.301	0.029
Mean	0.363	0.008
Median	0.341	0.002
Root mean squared	0.325	0.018
Uniformity	0.274	0.047
Id	0.274	0.047
Idm	0.274	0.047
Joint energy	0.320	0.020
Joint entropy	–0.277	0.045
Maximum probability	0.282	0.041
Long run emphasis	0.287	0.037
Run length non-uniformity normalized	–0.271	0.049
Run percentage	–0.285	0.039
Run variance	0.296	0.032
Short run emphasis	–0.285	0.039
Size zone non-uniformity normalized	0.357	0.009
Small area emphasis	0.339	0.013
MVI		
None	–	–

CK-19, cytokeratin 19; GPC-3, Glypican-3; Id, inverse difference; Idn, inverse difference normalized; Idm, inverse difference moment; Idmn, inverse difference moment normalized; MVI, microvascular invasion; SWI, susceptibility weighted imaging.

Table 4 SWI-derived radiomics features which were significantly correlated with CK-7 status

Radiomics features	*r*	*P*
CK-7		
Entropy	–0.383	0.007
Interquartile range	–0.347	0.016
Mean absolute deviation	–0.350	0.015
Robust mean absolute deviation	–0.338	0.019
Uniformity	0.386	0.007
Variance	–0.347	0.016
Cluster prominence	–0.326	0.024
Cluster tendency	–0.332	0.021
Contrast	–0.395	0.005
Difference average	–0.383	0.007
Difference entropy	–0.377	0.008
Difference variance	–0.362	0.011
Id	0.401	0.005
Idm	0.404	0.004
Inverse variance	0.380	0.008
Joint energy	0.404	0.004
Joint entropy	–0.380	0.008
Maximum probability	0.423	0.003
Sum entropy	–0.365	0.011
Sum squares	–0.353	0.014
Dependence variance	0.293	0.043
Gray level variance	–0.347	0.016
Gray level non-uniformity normalized	0.380	0.008
Gray level variance	–0.338	0.019
Long run emphasis	0.365	0.011
Run length non-uniformity normalized	–0.335	0.020
Run percentage	–0.341	0.018
Run variance	0.359	0.012
Short run emphasis	–0.341	0.018
Gray level non-uniformity normalized	0.296	0.041
Complexity	–0.290	0.046
Contrast	0.293	0.043

CK-7, cytokeratin 7; SWI, susceptibility weighted imaging; Id, inverse difference; Idm, inverse difference moment.

studies aimed to explore the feasibility of simultaneously predicting multiple histopathologic characteristics of HCC via MRI image features. (2) Some important immuno-oncological indexes were hardly evaluated via image features like CK-7, GPC-3 and CK-19 and so on which play significant roles in prognostic prediction, making therapeutic decision and guiding clinical management. Belonging to heparan sulfate proteoglycans family, GPC-3 is a highly expressed molecules on the surface of HCC cells. Recently, it has become a star molecule tightly associated with the occurrence and development of HCC.[25] Previous researches signified that GPC-3 was a more powerful diagnostic marker compared to AFP.[25] Furthermore, due to the fact that GPC-3 is specifically overexpressed in HCC cells, a lot of investigators have developed a

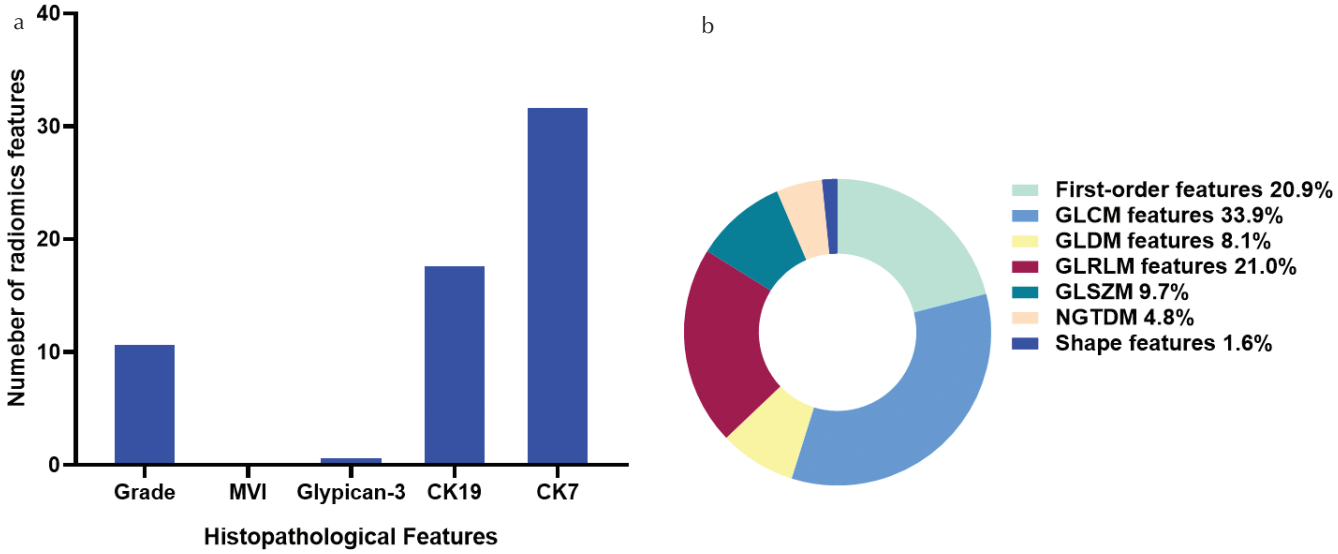

Fig. 5 Distribution of radiomics features. (**a**) The number of SWI-derived radiomics features showing significant correlation with different histopathological characteristics including histopathologic grade and status of MVI, CK-7, CK-19 and GPC-3 expression. (**b**) The distribution of all 63 radiomics features in seven radiomic feature categories. CK-7, cytokeratin 7; CK-19, cytokeratin 19; GPC-3, Glypican-3; MVI, microvascular invasion; SWI, susceptibility weighted imaging.

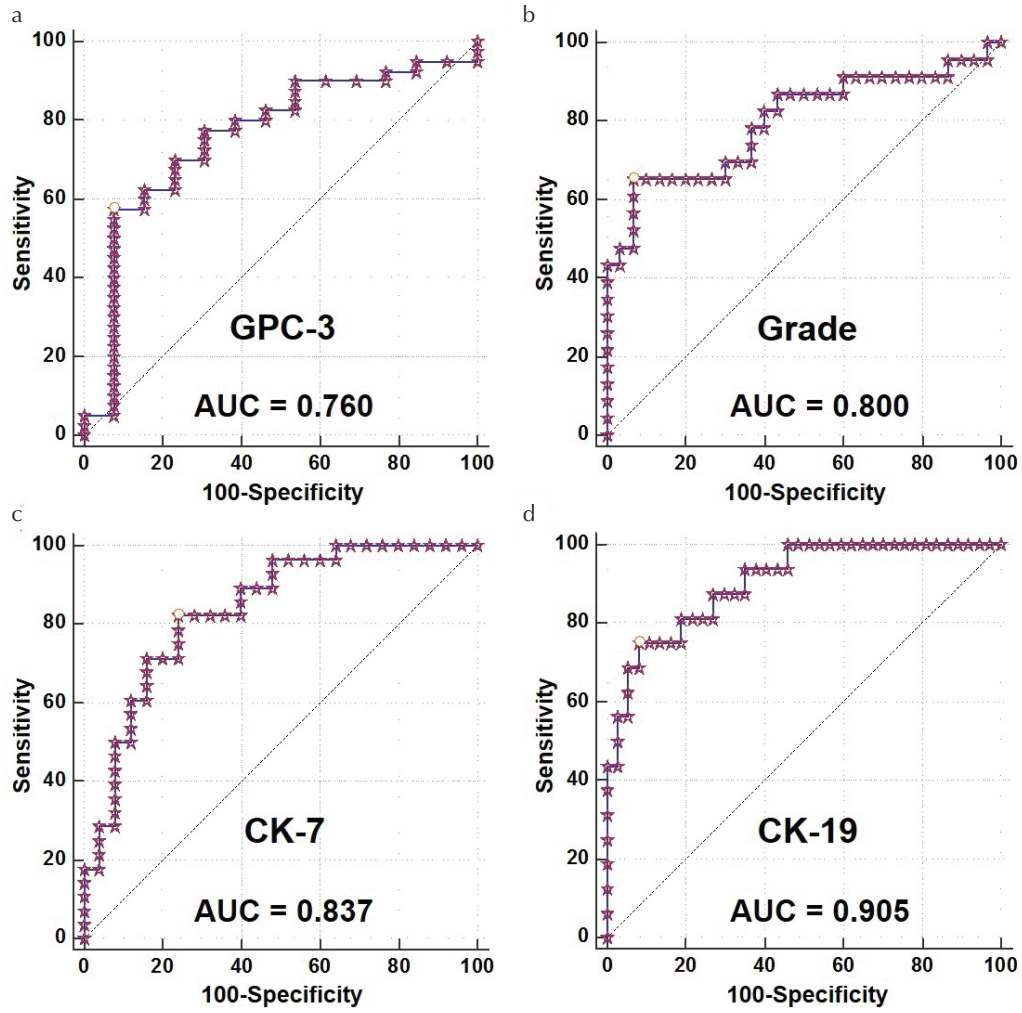

Fig. 6 ROC curves evaluation. The predictive power of logistic regression-based models for diagnosing patients with (**a**) positive GPC-3, (**b**) high grade, (**c**) positive CK-7 and (**d**) positive CK-19, respectively. *Note*: The values of AUCs were displayed in the figures. AUCs, areas under the curve; CK-7, cytokeratin 7; CK-19, cytokeratin 19; GPC-3, Glypican-3; ROC, receiver operating characteristic.

Table 5 Diagnostic performance indexes

	Sensitivity (%)	Specificity (%)	AUC	*P*	Youden index
LG_{CK-7}	82.1	76.0	0.837	***	0.581
LG_{CK-19}	75.0	91.9	0.905	***	0.669
LG_{Grade}	65.2	93.3	0.800	***	0.585
LG_{GPC-3}	57.5	92.3	0.760	**	0.498

Note: (1) Both ** and *** suggest that there is a significant difference between the AUC of diagnostic model and AUC of 0.500. ** indicates $P < 0.01$, *** indicates $P < 0.001$. (2) LG_{CK-7}, LG_{CK-19}, LG_{Grade} and LG_{GPC-3} are the abbreviations of logistic regression-based model for achieving diagnosing patients with different histopathological characteristics. AUCs, areas under the curve; LGCK-7, positive cytokeratin 7; LGCK-19, positive cytokeratin 19; LGGPC-3, positive Glypican-3; LGGrade, high grade hepatocellular carcinoma.

series of GPC-3-based targeting therapy strategy.[26–28] In addition, recent researches unveiled that HCCs with positive CK-19 signified the poorer prognosis, a higher rate of recurrence, and lymph node metastasis. Furthermore, many investigators have proposed CK-19 as an independent prognostic factor.[29,30] Similarly, the expression of CK-7 was reported to be associated with the aggressiveness of HCC.[3] Histopathologic grade, MVI and so on are also independent prognostic predictors of HCC.[5]

The results suggested that radiomics features derived from SWI were significantly correlated with the histopathologic grade, the expression status of CK-7, CK-19 and GPC-3, which meant that it was feasible to utilize the SWI-derived radiomics features for evaluating the histopathological features of HCC. The potential causes were as follows: (1) SWI applies the phase information to enhance the contrast of susceptibility change and is very sensitive for the "intrinsic contrast agents" such as deoxygenated hemoglobin, deposited iron and more. As a result, SWI is able to visualize some pathological changes including nodular dysplasia, hyper-vascularity, hemorrhage, even some specific morphological patterns such as the mosaic pattern of HCC.[20,31] Above pathological changes are also correlated with the occurrence and development of HCC, which leads to an indirect correlation between the pathologic variations visualized by SWI and histopathological indexes studied in this research. For instance, Chen et al.[20] revealed that the intra-tumoral hemorrhage was associated with the invasion and metastasis of HCC. Yang et al.[32] suggested that vascularity quantified by intra-tumoral susceptibility signal (ITSS) in SWI can be an effective biomarker for evaluating the tumor aggressiveness. (2) The state-of-art radiomics technology provided an unprecedented opportunity for extracting the underlying quantitative insights of images. Conventional imaging-based diagnosis often relies on morphological changes observed with the naked eyes. However, observable morphological image changes in tumor caused by pathological changes often take a long time to appear. Thus, radiomics analysis is powerful for timely capturing and reflecting the potential pathological changes. In order to evaluate the tumor histopathology including grade, stage, molecular subtypes, genotype and so on, a great deal of researches have been performed via MRI radiomics features with fascinating predictive power.[33,34] (3) Based on the aforementioned points, significant correlations between histopathologic features of HCC and SWI-derived radiomics features were obtained with the assistance of unique image contrast of SWI and hundreds of quantitative radiomics parameters. However, none of the SWI-derived radiomics features was significantly correlated with the MVI status. Potential reasons were as follows: compared to "invaded micro-vessel" of patients with MVI which are always located in the adjacent liver tissue and portal vein, SWI is more sensitive for sensing the pathologic changes related to "macro-vessels" such as hypervascularity and hemorrhage.[31] As a result, SWI-derived features did not show significant correlation with MVI in this research. However, more pathologically relevant evidence needs to be mined in subsequent studies.

Interestingly, there were most radiomics features showing significant correlations with the expression of two cytokeratin-family molecules including CK-7 and CK-19. Both CK-7 and CK-19 normally expressed in cholangiocytes in comparison to CK-8 and CK-18 normally expressed in hepatocytes. Moreover, CK-7 and CK-19 are also expressed in hepatic progenitor cells. Growing evidence shows that HCCs are not all originated from hepatocytes. Some HCCs developed from cholangiocytes and hepatic progenitor cells display the positive expression of CK-7 and CK-19 and are accompanied by the poor prognosis and aggressive biological behavior.[3,30] The biological basis of that there were most radiomics features showing significant correlations with the expression of CK-7 and CK-19 were as follows: the expression of CK-7/CK-19 were more associated with variations of some "intrinsic contrast agents" of SWI containing deposited iron and hemoglobin. Choi et al.[2] found that HCCs with positive CK-19 had a higher rate of multifocal nodular confluent compared to HCCs with negative CK-19 [CK19(+) vs. CK19(−): 5.3% vs. 2.5%]. Besides, HCCs with positive CK-19 were always accompanied by the intra-tumoral hemorrhage (60.5%) compared to HCC with negative CK-19 (40.7%).[2] According to the widely-reported application of SWI, the sensitivity of visualizing the hemorrhage, nodule,

hypervascularity and so on serves as the most prominent advantage of SWI.[19,35] Thus, in this research, most radiomics features showed significant correlations with the expression of CK-7 and CK-19.

SWI derived NGTDM_contrast, GLDM_dependence non-uniformity normalized, first-order_10th percentile and GLCM_maximum probability were most relevant parameters for histopathologic grade, GPC-3, CK-19 and CK-7, respectively. According to the mathematical definitions, except first-order_10th percentile, all of the above features were able to quantify the "image heterogeneity" based on calculating the correlation between the gray levels of two points in a certain distance and a certain direction in the image to reflect the comprehensive information of the image in the direction, interval, amplitude of change and speed of change. During the routine clinical practice, the most widely-utilized quantitative image features were the first-order features such as mean value, median value and so on. Among 62 features significantly correlated with histopathologic indexes, only 20.9% of features belonged to the category of first-order features, which meant at least 79.1% of features belonged to the category which were usually "ignored" and "wasted" during daily time. Based on aforementioned points, it was valuable to extract the radiomics features underlying qualitative image manifestations for clinical application.

Our results also preliminarily evaluated the diagnostic performance of different models based on logistic regression with SWI-derived radiomics features as independent variables. The results indicated HCCs with high histopathologic grade, positive CK-19, positive CK-7 and positive GPC-3 can be diagnosed with satisfying accuracy. Specifically, the AUC of model for diagnosing patients with positive CK-19 was more than 0.900. In addition, the AUCs of models for diagnosing patients with positive GPC-3, positive CK-7 and high histopathologic grade were also around 0.800. Above results further proved that: (1) some intrinsic "contrast agents" of SWI can be utilized for indirectly characterizing other histopathologic changes. (2) Integrating multiple radiomics features was meaningful for establishing powerful diagnostic models.

There were also some limitations should be acknowledged. First, the sample size was relatively small in this retrospective study. Moreover, because of the small sample size, internal cross-validation and external validation were not performed, which may resulted in the possible overfitting. Second, only five histopathologic features were evaluated due to the incomplete pathologic results of other indexes such as CD-31, CD-10, vascular endothelial growth factor (VEGF) and so on. More histopathologic indexes should be incorporated into the subsequent study.

Conclusion

In conclusion, this research suggested that extracting the radiomics features from SWI images was feasible to evaluate multiple histopathologic indexes of HCC.

Conflicts of Interest

The authors declare that they have no conflicts of interest.

Supplementary Information

Supplementary Fig. 1 is available online.

Supplementary Fig. 1

H&E stained histopathologic photomicrograph (×200) of one patient whose MR images are displayed in Figure 2 (MVI status: positive). Note: 1) Yellow arrow indicates the MVI. 2) Tumor edge was selected as the FOV. FOV, field of view; H&E, hematoxylin and eosin; MVI, microvascular invasion.

References

1. Bray F, Ferlay J, Soerjomataram I, Siegel RL, Torre LA, Jemal A. Global cancer statistics 2018: GLOBOCAN estimates of incidence and mortality worldwide for 36 cancers in 185 countries. CA Cancer J Clin 2018; 68: 394–424.
2. Choi SY, Kim SH, Park CK, et al. Imaging features of gadoxetic acid-enhanced and diffusion-weighted MR imaging for identifying cytokeratin 19-positive hepatocellular carcinoma: a retrospective observational study. Radiology 2018; 286:897–908.
3. Santos NP, Oliveira PA, Arantes-Rodrigues R, et al. Cytokeratin 7/19 expression in N-diethylnitrosamine-induced mouse hepatocellular lesions: implications for histogenesis. Int J Exp Pathol 2014; 95:191–198.
4. Filmus J, Capurro M. Glypican-3: a marker and a therapeutic target in hepatocellular carcinoma. FEBS J 2013; 280:2471–2476.
5. Wang WT, Yang L, Yang ZX, et al. Assessment of microvascular invasion of hepatocellular carcinoma with diffusion kurtosis imaging. Radiology 2018; 286:571–580.
6. Woo S, Lee JM, Yoon JH, Joo I, Han JK, Choi BI. Intravoxel incoherent motion diffusion-weighted MR imaging of hepatocellular carcinoma: correlation with enhancement degree and histologic grade. Radiology 2013; 270:758–767.
7. Low HM, Choi JY, Tan CH. Pathological variants of hepatocellular carcinoma on MRI: emphasis on histopathologic correlation. Abdom Radiol 2019; 44:493–508.
8. Yoo EY, Nam SY, Choi HY, Hong MJ. Agreement between MRI and pathologic analyses for determination of tumor size and correlation with immunohistochemical factors of invasive breast carcinoma. Acta Radiol 2018; 59:50–57.
9. Lee SJ, Mahoney MC, Khan S. MRI features of stromal fibrosis of the breast with histopathologic correlation. AJR Am J Roentgenol 2011; 197:755–762.
10. Burton S, Brown G, Daniels I, et al. MRI identified prognostic features of tumors in distal sigmoid, rectosigmoid, and upper rectum: treatment with radiotherapy and chemotherapy. Int J Radiat Oncol Biol Phys 2006; 65:445–451.

11. Haacke EM, Xu Y, Cheng YC, Reichenbach JR. Susceptibility weighted imaging (SWI). Magn Reson Med 2004; 52: 612–618.
12. Gillies RJ, Kinahan PE, Hricak H. Radiomics: images are more than pictures, they are data. Radiology 2016; 278:563–577.
13. Wang W, Gu D, Wei J, et al. A radiomics-based biomarker for cytokeratin 19 status of hepatocellular carcinoma with gadoxetic acid–enhanced MRI. Eur Radiol 2020; 30: 3004–3014.
14. Feng J, Zhu R, Chang C, et al. CK19 and Glypican 3 expression profiling in the prognostic indication for patients with HCC after surgical resection. PLoS One 2016; 11:e0151501.
15. Wang YL, Zhu ZJ, Teng DH, Yao Z, Gao W, Shen ZY. Glypican-3 expression and its relationship with recurrence of HCC after liver transplantation. World J Gastroenterol 2012; 18:2408–2414.
16. Choi JY, Kim MJ, Park YN, et al. Gadoxetate disodium–enhanced hepatobiliary phase MRI of hepatocellular carcinoma: correlation with histological characteristics. AJR Am J Roentgenol 2011; 197:399–405.
17. Matsuura S, Aishima S, Taguchi K, et al. 'Scirrhous' type hepatocellular carcinomas: a special reference to expression of cytokeratin 7 and hepatocyte paraffin 1. Histopathology 2005; 47:382–390.
18. van Griethuysen JJM, Fedorov A, Parmar C, et al. Computational radiomics system to decode the radiographic phenotype. Cancer Res 2017; 77:e104–e107.
19. Li RK, Zeng MS, Rao SX, et al. Using a 2D multibreath-hold susceptibility-weighted imaging to visualize intratumoral hemorrhage of hepatocellular carcinoma at 3T MRI: correlation with pathology. J Magn Reson Imaging 2012; 36:900–906.
20. Chen W, DelProposto Z, Liu W, et al. Susceptibility-weighted imaging for the noncontrast evaluation of hepatocellular carcinoma: a prospective study with histopathologic correlation. PLoS One 2014; 9:e98303.
21. Kim HG, Choi JW, Han M, Lee JH, Lee HS. Texture analysis of deep medullary veins on susceptibility-weighted imaging in infants: evaluating developmental and ischemic changes. Eur Radiol 2020; 30:2594–2603.
22. Zhou Y, Wang X, Xu C, et al. Mass-forming intrahepatic cholangiocarcinoma: can diffusion-weighted imaging predict microvascular invasion? J Magn Reson Imaging 2019; 50:315–324.
23. Li Y, Yan C, Weng S, et al. Texture analysis of multi-phase MRI images to detect expression of Ki67 in hepatocellular carcinoma. Clin Radiol 2019; 74:813.e819–813.e827.
24. Shan Q, Chen J, Zhang T, et al. Evaluating histologic differentiation of hepatitis B virus-related hepatocellular carcinoma using intravoxel incoherent motion and AFP levels alone and in combination. Abdom Radiol 2017; 42:2079–2088.
25. Guo M, Zhang H, Zheng J, Liu Y. Glypican-3: a new target for diagnosis and treatment of hepatocellular carcinoma. J Cancer 2020; 11:2008–2021.
26. Nishida T, Kataoka H. Glypican 3-targeted therapy in hepatocellular carcinoma. Cancers (Basel) 2019; 11:1339.
27. Shimizu Y, Suzuki T, Yoshikawa T, Endo I, Nakatsura T. Next-generation cancer immunotherapy targeting glypican-3. Front Oncol 2019; 9:248.
28. Fu Y, Urban DJ, Nani RR, et al. Glypican-3-specific antibody drug conjugates targeting hepatocellular carcinoma. Hepatology 2019; 70:563–576.
29. Sun DW, Zhang YY, Sun XD, et al. Prognostic value of cytokeratin 19 in hepatocellular carcinoma: a meta-analysis. Clin Chim Acta 2015; 448:161–169.
30. Wang ZS, Guo WD, Wu LQ, et al. Use of cytokeratin-19 concentration to assess early recurrence and prognosis of hepatitis B virus-related hepatocellular carcinoma following radical resection in patients with a low serum alpha-fetoprotein concentration. PLoS One 2015; 10:e0142727.
31. Chang SX, Li GW, Chen Y, et al. Characterizing venous vasculatures of hepatocellular carcinoma using a multi-breath-hold two-dimensional susceptibility weighted imaging. PLoS One 2013; 8:e65895.
32. Yang S, Lin J, Lu F, Han Z, Fu C, Gu H. Use of ultrasmall superparamagnetic iron oxide enhanced susceptibility weighted imaging and mean vessel density imaging to monitor antiangiogenic effects of sorafenib on experimental hepatocellular carcinoma. Contrast Media Mol Imaging 2017; 2017:9265098.
33. Wang J, Wu CJ, Bao ML, Zhang J, Wang XN, Zhang YD. Machine learning-based analysis of MR radiomics can help to improve the diagnostic performance of PI-RADS v2 in clinically relevant prostate cancer. Eur Radiol 2017; 27:4082–4090.
34. Zhang X, Xu X, Tian Q, et al. Radiomics assessment of bladder cancer grade using texture features from diffusion-weighted imaging. J Magn Reson Imaging 2017; 46:1281–1288.
35. Yang SH, Lin J, Lu F, et al. Contrast-enhanced susceptibility weighted imaging with ultrasmall superparamagnetic iron oxide improves the detection of tumor vascularity in a hepatocellular carcinoma nude mouse model. J Magn Reson Imaging 2016; 44:288–295.